Kemppainen, Reko; Suilamo, Sami; Tuokkola, Terhi; Lindholm, Paula; Deppe, Martin H.; Keyriläinen, Jani

Magnetic resonance-only simulation and dose calculation in external beam radiation therapy

Published in:
Acta Oncologica

DOI:
10.1080/0284186X.2017.1293290

Published: 04/05/2017

Document Version
Peer-reviewed accepted author manuscript, also known as Final accepted manuscript or Post-print

Please cite the original version:
Kemppainen, R., Suilamo, S., Tuokkola, T., Lindholm, P., Deppe, M. H., & Keyriläinen, J. (2017). Magnetic resonance-only simulation and dose calculation in external beam radiation therapy: a feasibility study for pelvic cancers. *Acta Oncologica*, *56*(6), 792-798. https://doi.org/10.1080/0284186X.2017.1293290

Magnetic Resonance-Only Simulation and Dose Calculation in External Beam Radiation Therapy: A Feasibility Study for Pelvic Cancers

Background

The clinical feasibility of using pseudo-computed tomography (pCT) images derived from magnetic resonance (MR) images for external bean radiation therapy (EBRT) planning for prostate cancer patients has been well demonstrated. This paper investigates the feasibility of applying an MR-derived, pCT planning approach to additional types of cancer in the pelvis.

Materials and Methods

Fifteen patients (five prostate cancer patients, five rectal cancer patients and five gynaecological cancer patients) receiving EBRT at Turku University Hospital (Turku, Finland) were included in the study. Images from an MRCAT (Magnetic Resonance for Calculating ATtenuation, Philips, The Netherlands) pCT method were generated as part of a clinical MR-simulation procedure. Dose calculation accuracy was assessed by comparing the pCT based calculation with a CT-based calculation. In addition, the degree of geometric accuracy was studied.

Results

The median relative difference of PTV mean dose between CT and pCT images was within 0.8% for all tumour types. When assessing the tumour site specific accuracy, the median [range] relative dose differences to the PTV mean were 0.7 [-0.11;1.05]% for the prostate cases, 0.3 [-0.25;0.57]% for the rectal cases and 0.09 [-0.69;0.25]% for the gynaecological cancer cases. System induced geometric distortion was measured to be less than 1 mm for all PTV volumes and the effect on the PTV median dose was less than 0.1%.

Conclusions

According to the comparison, using pCT for clinical EBRT planning and dose calculation in the three investigated types of pelvic cancers is feasible. Further studies are required to demonstrate the applicability to a larger cohort of patients.

Keywords: Radiotherapy, MRI treatment planning, pelvic cancer, dose calculation, geometric accuracy

Introduction

Computed tomography (CT) is currently the primary imaging modality for providing anatomical and tissue density information for external beam radiation therapy (EBRT) planning of prostate, rectal and gynaecological cancers. Magnetic resonance imaging (MRI) is widely used as a supplement to CT imaging in the planning of EBRT for pelvic cancers. The major advantages of MRI over CT are primarily better soft tissue contrast, which results in more accurate gross tumour volume (GTV) and organ at risk (OAR) delineation, lower inter-observer variability, better organ at risk (OAR) visibility, and better regional lymph node characterization [1]. Additional benefits include the usage of non-ionizing radiation and the versatility of existing imaging methods for cancer type or organ specific imaging methods [1].

A major drawback of multi-modality imaging in radiation therapy (RT) is the registration errors introduced when images from two or more imaging modalities are registered and fused [2]. Recent advances in the use of MRI in RT promise to eliminate this registration error by using only MR images for planning and dose calculation in EBRT of prostate [3–7] and brain [8,9]. In an MR-only workflow, so-called pseudo-CT images are generated from the MR images, providing tissue density information for dose calculation and reference images for patient position verification at the linear accelerator. However, despite the benefits of MR-based RT planning, it has not been investigated if it is possible to use existing pseudo-CT methods for other cancer types in the pelvic anatomy [1,10,11]. The pseudo-CT methods suitable for prostate may not be directly applicable to other pelvic targets due to the larger treatment volumes that are characteristic of pelvic tumours in general.

The geometric accuracy of images used in RT directly affects the required treatment margins and treatment outcomes of EBRT [12]. Consequently, geometric

accuracy of MRI has been studied in several publications and also reviewed recently [12]. However, a major limitation of previous studies has been that they only consider volumes relevant for a dual-modality workflow, whereby MR-images are registered to a planning CT. The accuracy of the full body contour is relevant in the context of an MR-only workflow due to its direct impact on dose calculation accuracy. Thus, we find it important to study the effect of geometric distortions on dose calculation accuracy, especially for the large PTV volumes typically treated in pelvic cancers.

The aim of this study was to evaluate the feasibility of an existing MR-only method in terms of dose calculation and geometric accuracy in EBRT for the pelvic area in general. The method is singularly used for prostate cancer, presently the only indication included in the labelling of this method. Since large target volumes are typically treated in gynaecological and rectal cancer patients, both system-related geometric distortion and patient-induced distortion were evaluated in the pelvic anatomy in order to quantify their impact on the dose planning and calculation accuracy.

Materials and Methods

Study design and image acquisition

The study cohort consisted of 15 consecutive pelvic cancer patients (five prostate, five rectal and five gynaecological) treated with EBRT at the Department of Oncology and Radiotherapy of Turku University Hospital in Turku, Finland. The mean (±SD) age was 74.3 (±4.8), 69.2 (±12.8) and 72.8 (±8.3) years and mean (±SD) weight was 91.4 (±21.7), 73.8 (±8.6) and 74.4 (±18.3) kg for the prostate, rectal and gynaecological groups. In the prostate cancer group, the PTV (volume mean (±SD) was 410 (±520) cm^3) included prostate, seminal vesicles and, for two patients, extra capsular

tumour extension was detected from the MR-images. For the rectal cancer group, the PTV (volume mean (±SD) was 1530 (±410) cm^3) was contoured according to clinical practice for preoperative EBRT of rectal cancer. For three out of the five gynaecological patients, the PTV (volume mean (±SD) was 1910 (±990) cm^3) included the primary tumour, the regional lymph nodes and, when applicable, other likely volumes of spread disease.

In pelvic cancer, gross tumour volumes (GTVs), including both the primary tumour and involved lymph nodes, were delineated in the MR images, and CTV was created by adding 5-15mm to GTVs in order to include subclinical or microscopic extensions of the disease. CTV also included regional lymph nodes at high risk for the spreading of microscopic cancer. PTV was then created by adding 10-15mm margins to CTV. GTV, CTV. PTV determinations were performed according to international guidelines on treating prostate, rectal, or gynaecological cancer, respectively. Two gynaecological and one prostate cancer patient received postoperative RT, and for those patients a postoperative tumour bed was included in the CTV. The time in between the CT and the MR simulations was less than one day for all patients. The manufacturer's 3D gradient non-linearity correction algorithm was used in all the MR images.

CT simulation images were acquired using an Aquilion LB (Toshiba Corp., Tokyo, Japan) scanner with 2-mm-thick slices, 1×1 mm^2 in-plane resolution and 120 kV tube voltage. MR images were recorded with the Ingenia 1.5T HP (Philips Medical Systems International B.V., Best, The Netherlands) scanner. For all patients, a transaxial T1-weighted three-dimensional (3D) mDIXON sequence [13] (resolution of 1.04×1.04×2.50 mm^3) covering the full body contour was acquired and used as a source for MRCAT (Magnetic Resonance for Calculating ATtenuation, Philips, Vantaa, Finland) images. The MR imaging time was less than 200 seconds for all patients, who

were positioned similarly during the imaging for CT and MR simulation. In the MR scan, patients were placed in a supine position on a flat RT couch top and an anterior MR-coil was placed above the imaging volume using a coil holder provided by the manufacturer.

MRCAT pseudo-CT generation

In the pCT generating algorithm, CT-like density maps were computed from the mDIXON MR-images in a two-step approach (see online Supplementary material for more detailed description of pCT generation). In the first step, the content of the MR image was categorized into five classes. In the second step, each voxel was assigned the following HU values: air (-968 HU), fat (-86 HU), water-rich tissue (42 HU), spongy bone (198 HU), and compact bone (949 HU). The densities used for dose calculation were then obtained from tabulated calibration values provided by the manufacturer and were based on the combination of average population values and values cited in the literature [14].

RT Treatment planning and image processing

Pinnacle^3 (version 9.10. Philips Medical Systems Inc., Fitchburg, WI, USA) treatment planning system (TPS) was used for generating and calculating the plans for this study. All clinical plans were originally done in Eclipse (version 13.6, Varian Medical Systems Oy, Helsinki, Finland) TPS and exported to Pinnacle^3, where the clinical plans were re-optimized using the original contours and a volumetric modulated arc therapy (VMAT) technique with two arcs. Planning was performed first using pCT images and clinical contours. The plans were then copied to the planning CT-image using identical planning parameters. The copied plan was recalculated based on the CT

image in Pinnacle^3 TPS using an adaptive convolution algorithm. The CT-to-density calibration curve was based on a recent calibration with the RMI 465 (Gammex Inc., Middleton, WI, USA) phantom. The pCT-specific calibration curve provided by the manufacturer was used for pCT-based calculations.

In order to avoid confounding factors in dose comparison, the original CT was first deformable-registered to the pCT source image (called CT_DIR) using Mirada (Mirada Medical Ltd., Oxford, UK) medical imaging software. The deformable registration was required since differences in the body outline would have otherwise caused dose differences that were not related to the performance of the pCT. Furthermore, it allows compensation of bladder and rectum filling differences and inner organ movement. An example of deformable registration can be seen in Figure S2 in the online Supplementary material.

The deformable image registration may bias the dose comparison results since MRI-related geometric distortions are not taken into account due to the body outline matching between pCT and CT images [12,15]. Furthermore, geometric inaccuracies may take place also in PTVs and OARs further away from the isocentre of the MR. In order to assess the impact of the MR-system's geometric accuracy on RT planning, another plan (called CT_DIR_C) where all structures were corrected according to measured system's geometric distortion was created (see below for a description of distortion measurement). This allowed the dose calculation discrepancies originating purely from the geometric inaccuracies to be studied independently from other sources, such as density differences.

Evaluation of dose calculation accuracy

Dose volume histogram (DVH) curves and gamma differences were analysed for any changes between pCT- and CT-based plans. Relevant PTV's DVH-metrics were selected to reflect the near maximum ($D_{2\%}$) and near minimum ($D_{98\%}$) values. For the OARs investigated in this study, i.e., rectum and bladder, the DVH-comparison dose of $D_{35\%}$ was tabulated. In addition, the differences in the median of mean doses to PTVs and OARs were calculated. In order to investigate the impact of tumour type to pCT performance, statistical analysis was performed to assess the significance of the differences between the prostate groups and the other two groups. The rationale for the statistical analysis is that the performance of pCT has been demonstrated for prostate EBRT and if no significant differences are found in the comparison to rectal and gynaecological targets, such as result would indicate clinical feasibility.

In addition to DVH comparison, the dose distributions between pCT and planning CT were compared by means of 3D gamma analysis using VeriSoft (version 6.1, PTW-Freiburg, Freiburg, Germany) treatment plan verification software. Doses below 30% of the maximum dose in the calculated volume were excluded from the analysis. The statistical tests were performed to determine if there is a significant difference between clinical pCT for prostate and pCT for the other pelvic areas (rectal and gynaecological cancers).

All dose differences are given as relative differences between the CT-based and pCT-based plans that can be formulated as (pCT-CT)/CT. Thus, positive values indicate dose deficiency if the treatment and dose calculation were based on pCT.

Assessment of geometric fidelity

Geometric distortions can be caused by both the MR system and the patient [12]. In this study, a large 3D phantom was used to measure the system-induced geometric distortions arising from gradient field non-linearity and static magnetic field (B0) inhomogeneity. In addition, patient-induced geometric distortion was assessed by calculating a B0 inhomogeneity map from two-phase images of a dual-echo fast field-echo (FFE) image as suggested by Baldwin *et al.* and Stanescu *et al.* [16,17]. The imaging parameters were as follows: TE1 of 1 ms, TE2 of 5.6 ms, TR of 6.8 ms, slice thickness of 4 mm and pixel size of 1x1 mm^2. Since the measured distortion originates from both the patient and the system, the patient-induced distortion was assessed in the neighbourhood of the MR system's isocentre, where system-related B0 inhomogeneity was the smallest. The phase images were unwrapped using an algorithm developed by Jenkinson *et al.* [18] . For the patient-induced distortion assessment, the additional dual-echo scan was included to the hospital's clinical MR protocol for a group of four patients.

The large FOV-3D phantom consists of seven acrylic plates with inter-plate distances of 65 mm. Each plate contains 240 fiducial markers placed in a regular grid with inter-fiducial distances of 25 mm. The phantom was scanned with a T1-weighted FFE sequence using the same MR scanner type that was used for the generation of the pCT images. The imaging parameters were as follows: FOV of 560×560×400 mm^3, acquisition voxel size of 1.5×1.5×2.0 mm^3, TE/TR of 3.4/6.7 ms and water-fat shift of 0.5 mm. The error as a function of the location inside the MR scanner was determined by comparing the fiducial locations to the known phantom grid. In order to assess the impact of geometric distortions to RT, the 3D distortion map was interpolated to the pCT image grid of the individual patients. The distortion map was then used for the

geometric correction of the RT structures. The corrected structures were created as DICOM RT structure sets using Matlab (version R2016b, The MathWorks Inc., Natick, MA, USA) mathematical computing software and imported to Pinnacle^3 TPS for dose calculation. The original CT_DIR plan was copied (the new plan is called CT_DIR_C) and the structures were replaced with the geometrically corrected structures. Finally, the impact on dose calculation was simulated by using the density override in Pinnacle, so that volume outside the distortion-corrected body outline was assigned as air and the volume inside the corrected outline was assigned as water for voxels for which there was air in the uncorrected image.

Statistical analysis

Statistical analysis was conducted using Minitab (version 17, Minitab Inc., State College, PA, USA) numerical analysis software. The data were analysed for statistical difference with the non-parametric Mann–Whitney U-test. This test was chosen due to the fact that the same data were not used for both treatment options and normality could not be guaranteed. For the statistical difference, 95% confidence level was required ($p < 0.05$).

Results

Dose comparison

The mean (± SD) relative dose difference in PTV mean dose computed over all 15 patients was 0.2 (± 0.5)% and the median of relevant PTV DVH-points was less than 0.9% for all studied tumour types, indicating good agreement between pCT and planning CT in terms of dose calculation accuracy. For the studied OARs, the median relative differences were less than 1.2% (see Table 1).

The gamma pass rates were high for all studied PTVs and pass criteria. The median pass rate was highest for the prostate patients and lowest for gynaecological patients. Although the differences between groups were small, statistically significant differences to the prostate group were found for the gamma criteria of 2% / 1 mm in both the rectal and the gynaecological groups. In addition, there was a significant difference in the gynaecological group when 2% / 2mm pass criteria were used. The results of the gamma analysis are shown in Table 2.

System's geometric accuracy

Geometric fidelity of the MR images was assessed for all patients and PTVs in the ROIs consisting of the clinical RT planning structures. An example of the analysis is illustrated in Figure 1, which demonstrates the contour distortions and ranges (minimum to maximum) and contours of the distortion map as a function of distance from the isocentre of the MR device for the gynaecological cancer patient that had the largest PTV in the cranial-caudal direction.

For all OAR structures, the distortion was measured to be less than 1 mm for all patients and PTVs (see illustration of the organ and disease specific figures in Figure 2). Furthermore, the maximum distortion in the body outline at which the radiation beam

enters the body was less than 2 mm for all prostate and rectal cancer patients. For one gynaecological patient, the body outline distortion was greater than 2 mm in the cranial end of the PTV. However, it can be seen in the standard deviation of the body outline distortion that the distortion was less than 2 mm for the majority of the outline.

Impact of geometric distortion to dose calculation accuracy

According to the results, the impact on dose calculation accuracy due to geometric distortions of the MR images was small. The changes in the PTV DVHs were negligible, the relative difference being less than 0.2% for all studied DVH points (see Table 3). The gamma-analysis was in line with the DVH-based analysis: pass rate was highest for prostate cancer patients and lowest for gynaecological cancer patients (see Table S1 in Supplementary material). The median pass rates were significantly different between prostate and gynaecological patients.

Patient-induced geometric distortions

Patient-induced geometric distortions were studied in the pelvis anatomy for four patients. In **Error! Reference source not found.**, an example of the magnitude of patient-induced distortion is given in axial plan near the isocentre of the MR device. Largest distortions were found near tissue-air interfaces (around rectum and near body outline). The distortions were found to be less than the pixel size of 1 mm for all studied patients.

Discussion

This work aimed at demonstrating the feasibility of using MRCAT pCT for the RT of pelvic cancers in terms of dosimetric and geometric accuracy. Our results show that the calculation accuracy is similar to reported in the literature. For example, Korhonen *et al.*

[3] have reported $D_{50\%}$ to be 0.3 (± 0.2)% for prostate EBRT, and we obtained 0.6 (± 0.5)%, 0.2 (± 0.4)% and -0.2 (± 0.5)% for prostate, rectal and gynaecological tumour patients respectively. Furthermore, Siversson *et al.* [4] have reported mean relative difference of 0.0 (±0.2)% and Kim *et al.* [5] 0.5% for PTV for EBRT of prostate. However, they are not fully comparable since in the reported studies the same CT scanner, calibration and dose calculation are used for both pseudo-CT method's development and its validation, and thus this may provide by far too optimistic results. Although no statistical significance was found between prostate and other cancers, the difference in DVH-points was almost significant and due to low power of the test (small sample size and heterogeneous demographics), the conclusions of similarity cannot be strongly considered.

Gamma analysis comparing the dose distributions of pCT and the reference planning-CT showed clinically acceptable pass rate for all cancer groups. The gamma pass rates (1% / 1 mm criteria) of 97.9, 97.5 and 96.9% for prostate, rectal and gynaecological groups, respectively, were well in line with results reported in the literature. Korhonen *et al.* [3] have reported a gamma pass rate of 95.7% and Kim *et al.*[5] 97.2% between pseudo-CT and planning-CT doses evaluated using the criteria of 1% / 1 mm for EBRT of prostate cancer.

According to literature, the geometric accuracy of 2 mm in ROI and 1 mm in PTV is desired for MR-guided RT [12]. We found that for all the patients the system-induced geometrical distortion was less than 1 mm for PTV and OAR volumes. In addition, the deformation of body contour was less than 2 mm for all except one gynaecological patient, when considering only the area at which the radiation beam enters the body. The impact of the body outline, PTV and OAR distortions on dose calculation accuracy was found to be clinically insignificant, the mean relative

difference of 0.2% being largest among all studied cancer groups. In Figure 2, however, one can see that the geometric distortion of body outline increases rapidly in the periphery of analysed volumes. This indicates that 30-cm-FOV in the cranial-caudal direction cannot be increased for larger PTVs without compromising the geometric accuracy.

Patient-induced distortions in transversal plane were assessed in the vicinity of MR device's isocentre for avoiding the contribution of system-induced B0 inhomogeneity. The largest distortions were found in air-tissue interfaces. The acceptable distortions were less than ± 0.5 mm for all studied patients being smaller than system-related distortions. When optimizing MR-sequences to be used in RT planning, the receiver bandwidth must be set high enough to avoid distortions of up to several millimetres [16,17]. Patient-induced geometric distortion originating from the susceptibility differences has been studied by Stanescu *et al.* [17]. For 1.5T system, the maximum distortion was 0.3 mm when a gradient strength of 20 mT/m was used. Since pCT source scan uses gradient strength of approximately 10 mT/m, results are in agreement with the values reported in the literature.

The system-induced geometric distortions are scanner dependent, and thus the results apply only to the scanner type and field strength used in this study. Additionally, the patient-induced distortions are sequence dependent and apply only for the studied sequences. Used 3D phantom for measuring the residual distortions after gradient non-linearity correction was considered as an object of known geometry. Therefore, the measures of geometric distortion may be overestimated due to any deviation from the assumed geometry which is not taken into account in the analysis. Deviations in the phantom geometry could be included into the analysis by using a CT scanner to obtain a geometrically accurate reference image. In our analysis, the measured residual

geometric distortion consists of system-related gradient and B0 distortions. In addition, the measured sequence dependent geometric distortion is a measure of both system and patient-induced B0 distortions. Thus, the system-related B0 distortions are measured in both the phantom and the patient experiments and their summation would double the impact of distortions originating from the main magnet. Our method can be considered adequate since the scope of this study was the assessment of clinical feasibility of using MRCAT pCT for RT of pelvic cancers, rather than providing a quantitative information of geometric distortions.

Currently, the cranial-caudal FOV of pCT image is limited to 300 mm that restricts its application in RT of wider pelvic cancers. Consequently, without increasing the imaging volume, the pCT can be used for RT treatment planning of primary pelvic cancers together with the regional lymph nodes, whereas it is not feasible for PTVs including para-aortic lymph nodes. At Turku University Hospital, around 10% of the PTVs for treating gynaecological cancer require larger a FOV than that is possible to calculate by way of the pCT method. Still, it would be feasible to treat the majority of pelvic cancers and overall prostate, rectal and gynaecological RT treatments constituted 36, 10 and 13% of all EBRT patients. The use of pCT in our clinic would enable MR-only simulation for around 60% of the patients being scanned with MR for RT.

The patient positioning at treatment device is based either on bone registration using orthogonal x-ray images and digitally reconstructed radiographs or on registration of the cone-beam CT and the planning CT. When pCT is used, only two soft-tissue HU-values are used, and thus the registration to the planning image may not be feasible. Robust registration might depend on continuous HU values for soft tissue [17,19]. The verification of pCT-based patient positioning requires further studies before its feasibility can be stated.

Increasing the FOV in the cranio-caudal direction remains a challenge in MRI since the geometric accuracy decreases rapidly farther away from the MR device's isocentre. Furthermore, motion blurring influenced by breathing in the abdomen causes artefacts in the mDIXON image, which may hamper accurate body outline detection. Recent development of MR sequences may address some of the above-mentioned challenges in the near future. Several academic institutions and industry are pursuing the technical advances aimed at in this issue, so it is very probable that over the next few years some solutions will be made commercially available, thus enabling easier utilization of the method on-site [20,21].

Judging by the results of this work, we conclude that the use of only four tissue classes is adequate to capture individual variance in body composition and to produce clinically acceptable accuracy in dose calculation for prostate, rectal and gynaecological cancer patients treated with EBRT. In addition, the geometric accuracy of the MR system used in the study was found to be sufficient for larger PTV, which is a necessity in an MR-only application for the pelvic area in general. Further studies are required to assess the feasibility of soft-tissue or bone-based patient positioning with pCT and to confirm our findings with a larger cohort of patients.

Disclosure of interest

Authors R. Kemppainen and M. Deppe are employed by Philips MR Therapy, Finland.

References

[1] Schmidt MA, Payne GS. Radiotherapy planning using MRI. Phys Med Biol 2015;60:R323–61. doi:10.1088/0031-9155/60/22/R323.

[2] Nyholm T, Nyberg M, Karlsson MG, Karlsson M. Systematisation of spatial uncertainties for comparison between a MR and a CT-based radiotherapy workflow for prostate treatments. Radiat Oncol 2009;4:54. doi:10.1186/1748-717X-4-54.

[3] Korhonen J, Kapanen M, Keyriläinen J, Seppälä T, Tenhunen M. A dual model HU conversion from MRI intensity values within and outside of bone segment for MRI-based radiotherapy treatment planning of prostate cancer. Med Phys 2014;41:11704. doi:10.1118/1.4842575.

[4] Siversson C, Nordström F, Nilsson T, Nyholm T, Jonsson J, Gunnlaugsson A, et al. Technical Note: MRI only prostate radiotherapy planning using the statistical decomposition algorithm. Med Phys 2015;42:6090–7. doi:10.1118/1.4931417.

[5] Kim J, Garbarino K, Schultz L, Levin K, Movsas B, Siddiqui MS, et al. Dosimetric evaluation of synthetic CT relative to bulk density assignment-based magnetic resonance-only approaches for prostate radiotherapy. Radiat Oncol 2015;10:239. doi:10.1186/s13014-015-0549-7.

[6] Andreasen D, Van Leemput K, Edmund JM. A patch-based pseudo-CT approach for MRI-only radiotherapy in the pelvis. Med Phys 2016;43:4742–52. doi:10.1118/1.4958676.

[7] Dowling JA, Lambert J, Parker J, Salvado O, Fripp J, Capp A, et al. An atlas-

based electron density mapping method for magnetic resonance imaging (MRI)-alone treatment planning and adaptive MRI-based prostate radiation therapy. Int J Radiat Oncol Biol Phys 2012;83:e5-11. doi:10.1016/j.ijrobp.2011.11.056.

[8] Andreasen D, Van Leemput K, Hansen RH, Andersen J a. L, Edmund JM. Patch-based generation of a pseudo CT from conventional MRI sequences for MRI-only radiotherapy of the brain. Med Phys 2015;42:1596–605. doi:10.1118/1.4914158.

[9] Hsu S-H, Cao Y, Lawrence TS, Tsien C, Feng M, Grodzki DM, et al. Quantitative characterizations of ultrashort echo (UTE) images for supporting air–bone separation in the head. Phys Med Biol 2015;60:2869–80. doi:10.1088/0031-9155/60/7/2869.

[10] Gwynne S, Mukherjee S, Webster R, Spezi E, Staffurth J, Coles B, et al. Imaging for target volume delineation in rectal cancer radiotherapy--a systematic review. Clin Oncol (R Coll Radiol) 2012;24:52–63. doi:10.1016/j.clon.2011.10.001.

[11] Dimopoulos J, Schard G, Berger D, Lang S, Goldner G, Helbich T, et al. Systematic evaluation of MRI findings in different stages of treatment of cervical cancer: potential of MRI on delineation of target, pathoanatomic structures, and organs at risk. Int J Radiat Oncol Biol Phys 2006;64:1380–8. doi:10.1016/j.ijrobp.2005.10.017.

[12] Weygand J, Fuller CD, Ibbott GS, Mohamed ASR, Ding Y, Yang J, et al. Spatial Precision in Magnetic Resonance Imaging-Guided Radiotherapy: The Role of Geometric Distortion. Int J Radiat Oncol 2016;95:1304–16. doi:10.1016/j.ijrobp.2016.02.059.

[13] Eggers H, Brendel B, Duijndam A, Herigault G. Dual-echo Dixon imaging with flexible choice of echo times. Magn Reson Med 2011;65:96–107. doi:10.1002/mrm.22578.

[14] Köhler M, Vaara T, Grootel M Van, Hoogeveen R, Kemppainen R, Renisch S. White paper: MR-only simulation for radiotherapy planning. Philips 2015:1–16.

[15] Walker A, Liney G, Metcalfe P, Holloway L. MRI distortion: Considerations for MRI based radiotherapy treatment planning. Australas Phys Eng Sci Med 2014;37:103–13. doi:10.1007/s13246-014-0252-2.

[16] Baldwin LLN, Wachowicz K, Fallone BG. A two-step scheme for distortion rectification of magnetic resonance images. Med Phys 2009;36:3917. doi:10.1118/1.3180107.

[17] Stanescu T, Wachowicz K, Jaffray D. Characterization of tissue magnetic susceptibility-induced distortions for MRIgRT. Med Phys 2012;39:7185–93. doi:10.1118/1.4764481.

[18] Jenkinson M. Fast, automated, N-dimensional phase-unwrapping algorithm. Magn Reson Med 2003;49:193–7. doi:10.1002/mrm.10354.

[19] Korhonen J, Kapanen M, Sonke J-J, Wee L, Salli E, Keyriläinen J, et al. Feasibility of MRI-based reference images for image-guided radiotherapy of the pelvis with either cone-beam computed tomography or planar localization images. Acta Oncol (Madr) 2015;54:889–95. doi:10.3109/0284186X.2014.958197.

[20] Walker A, Liney G, Holloway L, Dowling J, Rivest-Henault D, Metcalfe P.

Continuous table acquisition MRI for radiotherapy treatment planning: Distortion assessment with a new extended 3D volumetric phantom. Med Phys 2015;42:1982. doi:10.1118/1.4915920.

[21] Yang J, Cai J, Wang H, Chang Z, Czito BG, Bashir MR, et al. Four-Dimensional Magnetic Resonance Imaging Using Axial Body Area as Respiratory Surrogate : Initial Patient Results. Radiat Oncol Biol 2014;88:907–12. doi:10.1016/j.ijrobp.2013.11.245.

Figures

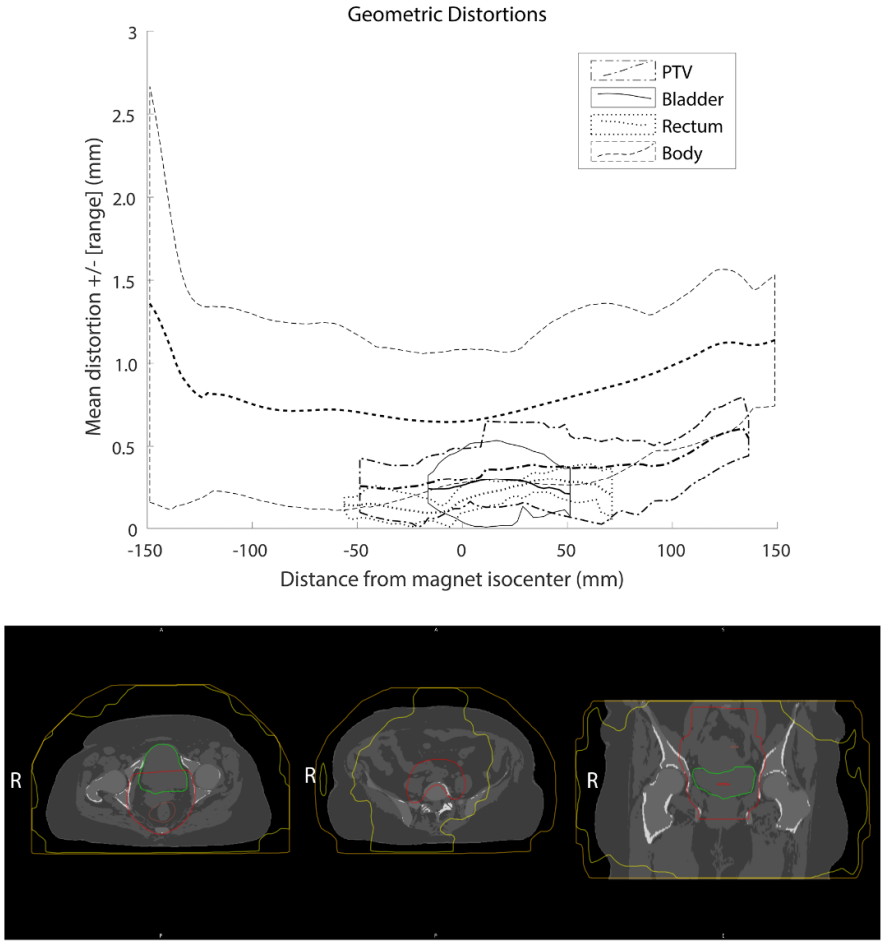

Figure 1: An example of geometric distortion for a patient receiving external beam radiation therapy (EBRT) for cervical cancer. Above: Mean and range of distortion for the body (dashed), planning target volume (PTV) (dash-dotted) and organs at risk (OAR) (solid=bladder and dotted=rectum) as function of distance from the magnet's isocentre along cranial-caudal direction. Below: illustration of the same plan in transversal (left:at the isocentre, middle 132 mm away from the isocentre) and coronal (right) planes with clinical structures and distortion contours of 1 mm (inner) and 2 mm (outer).

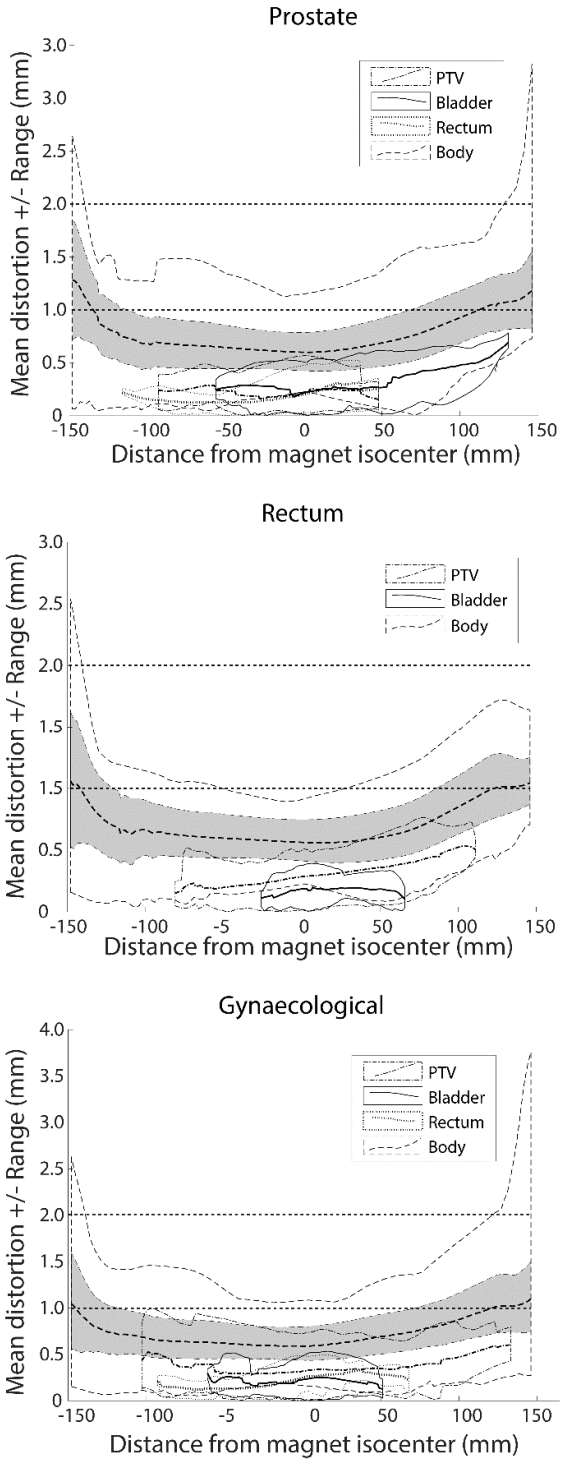

Figure 2: Population mean (± range) distortion per structure as a function of distance from the isocentre of the device along cranial-caudal direction. Dashed= Body outline, dash-dotted = planning target volume (PTV), dotted=Rectum and solid=Bladder. For the body structure the mean ± 1 SD is also given (see the darker area around the mean values). (PTV: planning target volume; SD: standard deviation).

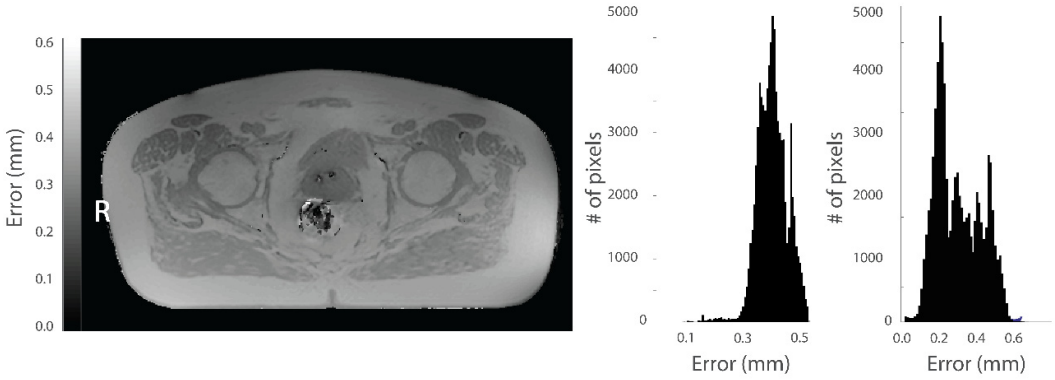

Figure 3: An example of distortion map with colour bar showing the amount of distortion (top), histogram of the error around the magnet isocentre (bottom left) for the example on top and histogram of geometric distortion for all four patients included to the analysis (bottom right).

Tables

Table 1: Median (min;max) relative difference (%) between MRCAT and CT_DIR-based plans for relevant dose volume histogram (DVH)-points and mean dose. Statistical tests were performed for equivalent median between prostate and rectal or gynaecological group, $p<0.05$ indicating statistically significant difference.

	Prostate	**Rectal**	**Gynaecological**
PTV			
Mean	0.73 (-0.11;1.05)	0.30 (-0.25;0.57), p=0.09	0.09 (-0.69;0.25), p=0.06
$D_{2\%}$	0.70 (0.53;0.46)	0.08 (-0.67;0.48), p>0.10	-0.20 (-1.23;0-06), p=0.04
$D_{50\%}$	0.56 (-0.11;1.04)	0.26 (-0.26;0.54), p>0.10	0.10 (-0.65;0.20), p=0.06
$D_{98\%}$	0.87 (-0.11;1.42)	0.57 (0.09;1.02), p>0.10	0.22 (-0.51;0.72), p>0.10
Rectum (OAR)			
Mean	0.23 (-0.19;1.25)	[N/A]	-0.14 (-1.10;0.23), p>0.10
$D_{35\%}$	0.45 (-0.63;1.78)	[N/A]	-0.19 (-1.00;0.62), p>0.10
Bladder (OAR)			
Mean	0.17 (-0.79;0.64)	-0.20 (-0.25;0.43), p>0.10	-0.45 (-0.75;0.13), p>0.10
$D_{35\%}$	-1.19 (-1.41;0.73)	0.24 (±-0.42;0.56), p>0.10	-0.24 (-0.65;0.02), p>0.10

Table 2: Results of gamma analysis (median pass rate (min;max). Statistical tests were performed for equivalent median between prostate and rectal or gynaecological group, $p<0.05$ indicating statistically significant difference.

	Prostate	Rectal	Gynaecological
Gamma criteria			
1% / 1mm	99.2 (93.8;100)	97.4 (96.4;99.0), p>0.10	97.3 (94.3;98.9), p>0.10
2% / 1mm	100 (99.5;100)	99.0 (98.7;99.8), p=0.03	98.5 (98.1;99.6), p=0.02
2% / 2mm	100 (99.8;100)	99.3 (99.1;100), p=0.06	99.2 (98.9;99.8), p=0.01

Table 3: Median (min;max) relative difference (%) between MRCAT and geometry-corrected CT plan (CT_DIR_C) plans for relevant dose volume histogram (DVH)-points and mean dose. Statistical tests were performed for equivalent median between prostate and rectal or gynaecological group, $p<0.05$ indicating statistically significant difference.

	Prostate	Rectal	Gynaecological
PTV			
Mean	0.10 (0.09;0.11)	0.06 (0.06;0.08), p=0.01	0.08 (0.05;0.10), p=0.09
$D_{2\%}$	0.08 (0.04;0.11)	0.09 (0.07;0.09), p>0.10	0.09 (0.04;0.09), p=0.02
$D_{50\%}$	0.10 (0.07;0.11)	0.07 (0.05;0.08), p=0.04	0.09 (0.05;0.09), p>0.10
$D_{98\%}$	0.12 (0.04;0.22)	0.10 (0.09;0.12), p>0.10	0.09 (-0.14;0.12), p>0.10
Rectum (OAR)			
Mean	-0.51 (-1.02;-0.1)	-	-0.02 (-0.18;0.08), p>0.10
$V_{35\%}$	-0.69 (-1.32;0.06)	-	0.04 (-0.29;0.07), p>0.10
Bladder (OAR)			
Mean	0.01 (-0.12;0.09)	-0.00 (-0.17;0.02), p>0.10	0.01 (-0.04;0.07), p>0.10
$V_{35\%}$	-0.07 (-0.18;0.08)	0.04 (-0.36;0.07), p>0.10	0.07 (0.03;0.09), p=0.06

PTV: planning target volume; OAR: organ at risk

Online Supplementary Material

Table S1: Results of gamma analysis (median pass rate (min;max)). Statistical tests were performed for equivalent median between prostate and rectal or gynaecological group, $p<0.05$ indicating statistically significant difference.

	Prostate	Rectal	Gynaecological
Gamma criteria			
0.5% / 0.5 mm	99.8 (99.2;99.9)	99.4 (99.3;99.9), p>0.10	98.7 (98.4;99.6), p=0.06
1% / 1 mm	100 (99.8;100)	99.8 (99.3;100), p>0.10	99.6 (99.4;99.9), p=0.04

MRCAT generation

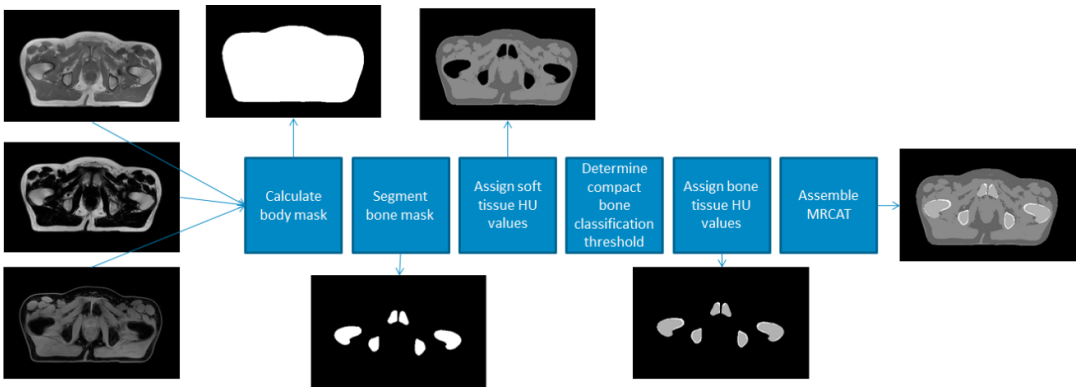

Figure S1: MRCAT generating algorithm pipeline. The three source images on left from mDIXON reconstruction (from top to bottom: inphase, fat and water images) are used as an input for the algorithm. HU: Hounsfield unit; MRCAT: magnetic resonance for calculating attenuation.

The classification of a certain voxel to a density class was determined by the following procedure. First, the body outline (skin) of the patient was determined: the voxels outside this outline were classified as air. Second, all bone structures inside the body were segmented using the multiple contrasts provided by the mDIXON scan. Both bone and outline segmentations employed a model-based approach trained on prostate cancer patients' and representative volunteers' image dataset. The model was adapted to the actual patient image using features (such as edges of grey values) found within the image, while at the same time, a constraint for the shape of the segmented structure

prevented the segmentation from being attracted to the wrong position [1]. The framework allowed modelling the organ shape in a flexible manner using local degrees of freedom for scaling, orientation, and shape-controlled deformation. Two models were used for pCT: an outline for background removal and a multi-step bone model for fine segmentation of all bony anatomy structures of the pelvis.

All voxels inside the body outline, except those from the bone segmentation, were considered as soft tissue. The soft tissue was further subdivided into water and fat by using the mDIXON fat and water images; the voxels with a higher fat content than that of water were classified as fat, whereas the voxels with higher water content than that of fat were classified as water. Voxels inside the bone segmentation are assumed to consist of either compact or spongy bone; the distinction is made based on the voxel intensity of the in-phase mDIXON image. The MRCAT algorithm is designed to segment all air cavities inside the body as soft-tissue. The choice is justified from dose calculation accuracy point of view since air cavities in the pelvis change their volume and appearance in short time intervals and can’t be considered stable.

Non-rigid registration procedure

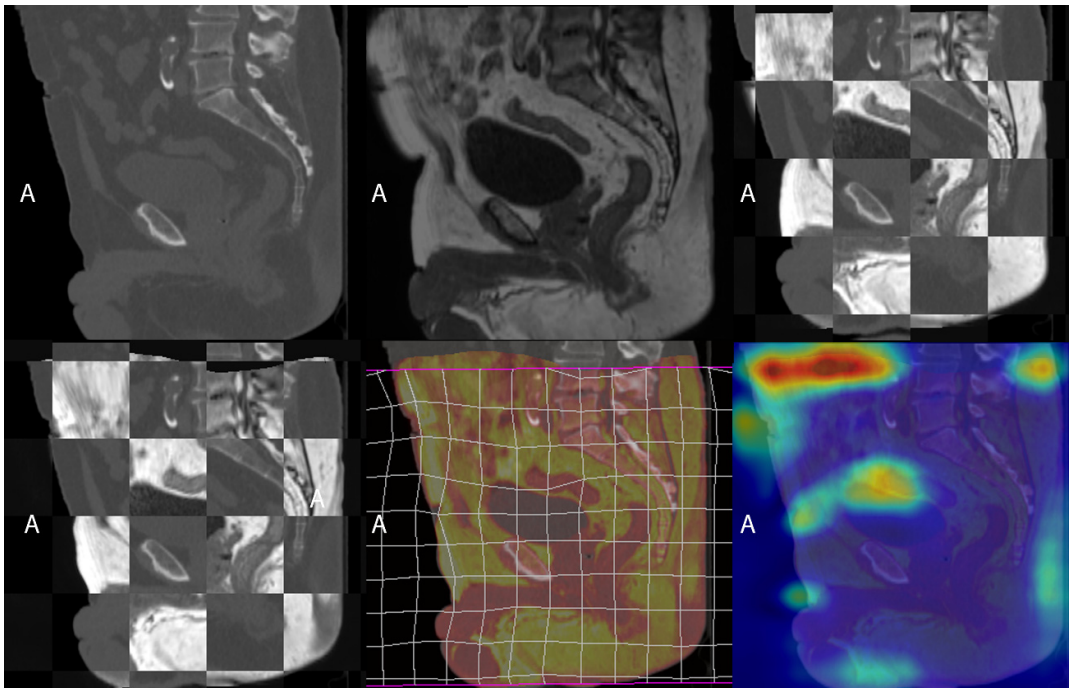

Figure S2: CT image registration to mDIXON inphase MR-image. Top from left to right: Original CT and inphase mDIXON images and their fusion showing skin outline and bladder differences. Bottom from left to right: CT and inphase fusion after deformable image registration and two illustrations showing the locations of largest deformations. (CT: computed tomography; MR: magnetic resonance).

[1] Ecabert O, Peters J, Schramm H, Lorenz C, Von Berg J, Walker MJ, et al. Automatic model-based segmentation of the heart in CT images. IEEE Trans Med Imaging 2008;27:1189–202. doi:10.1109/TMI.2008.918330.